Physics Letters B 818 (2021) 136384

Contents lists available at ScienceDirect

Physics Letters B

www.elsevier.com/locate/physletb

Diamagnetic and paramagnetic phases in low-energy quantum chromodynamics

Christoph P. Hofmann

Facultad de Ciencias, Universidad de Colima, Bernal Díaz del Castillo 340, Colima C.P. 28045, Mexico

ARTICLE INFO

Article history:
Received 15 March 2021
Received in revised form 5 May 2021
Accepted 20 May 2021
Available online 23 May 2021
Editor: B. Grinstein

ABSTRACT

While it is known that the QCD vacuum in a magnetic background exhibits both diamagnetic and paramagnetic characteristics in the low-energy domain, a systematic investigation of the corresponding phases emerging in the pion-dominated regime is still lacking. Here, within two-flavor chiral perturbation theory, taking into account the pion-pion interaction, we analyze the subtle interplay between zero- and finite-temperature portions in the magnetization and magnetic susceptibility. The dependence of the magnetic susceptibility on temperature and magnetic field strength in the paramagnetic and diamagnetic phase is non-monotonic. Our low-energy analysis complements lattice QCD that is currently operating at higher temperatures and stronger magnetic fields.

1. Introduction

Achieving a more quantitative understanding of the phases emerging in quantum chromodynamics (QCD) subjected to external magnetic fields, is a major theme in current strong interaction research. One objective is to gain more rigorous insights into the nonperturbative regime of QCD – or the standard model of particle physics in general. Apart from theoretical aspects such as the characterization of compact neutron stars (magnetic field strengths up to $10^{14}\,\mathrm{T}$ in their interior) or primordial magnetic fields in the early universe ($\lessapprox 10^{19}\,\mathrm{T}$), the problem is also phenomenologically relevant in view of heavy-ion collision experiments that probe the quark-gluon plasma ($\lessapprox 10^{16}\,\mathrm{T}$). Here we focus on the low-energy domain where magnetic fields are weak and temperatures are low compared to the chiral symmetry breaking scale $\Lambda_\chi \approx 1\,\mathrm{GeV}$ ($\Lambda_\chi^2 \approx 10^{16}\,\mathrm{T}$). It should be noted that the magnetic fields involved in heavy-ion collision experiments most likely never exceed the scale Λ_χ^2.

The thermomagnetic properties of QCD are described by the magnetization $\mathfrak{M}_{\mathrm{tot}}$ and the magnetic susceptibility χ_{tot}.[1] The classification of the QCD vacuum into diamagnetic or paramagnetic relies on the sign of the magnetic susceptibility, defined as the response of the magnetization with respect to the external magnetic field H,[2]

$$\chi_{\mathrm{tot}} = \frac{\mathrm{d}\mathfrak{M}_{\mathrm{tot}}}{\mathrm{d}|qH|}\,, \qquad \mathfrak{M}_{\mathrm{tot}} = -\frac{\mathrm{d}z_{\mathrm{tot}}}{\mathrm{d}|qH|}\,. \tag{1.1}$$

Here z_{tot} is the free energy density and q is the electric charge. Aside from lattice QCD simulations [1–13], alternative approaches to study $\mathfrak{M}_{\mathrm{tot}}$ and χ_{tot} rely on the Nambu-Jona-Lasinio model and extensions thereof [14–16], on the hadron resonance gas (HRG) model [17–19], and on yet other techniques [20–34]. Remarkably, a systematic investigation of the magnetic susceptibility within chiral perturbation (CHPT) – i.e., the low-energy effective field theory of QCD – appears to be lacking.

The overall picture that emerged from these studies is that the QCD vacuum behaves as a diamagnetic medium at low temperatures, while at higher temperatures, around $T \approx 110\,\mathrm{MeV}$, it evolves into a paramagnetic medium. The fact that χ_{tot} changes from negative into positive as temperature – or magnetic field strength – increase, can be traced back to various reasons. First, at low T, the physics of the

E-mail address: christoph.peter.hofmann@gmail.com.

[1] The magnetic susceptibility – much like the magnetization and the free energy density – contains a zero-temperature piece χ_0 and a purely finite-temperature portion χ_T. The subscript "tot" means that we refer to the sum of the two contributions: $\chi_{\mathrm{tot}} = \chi_0 + \chi_T$.

[2] In the literature, the term "magnetic susceptibility" usually refers to the limit $H \to 0$. In the present study, we also consider the magnetic susceptibility in nonzero magnetic fields.

https://doi.org/10.1016/j.physletb.2021.136384

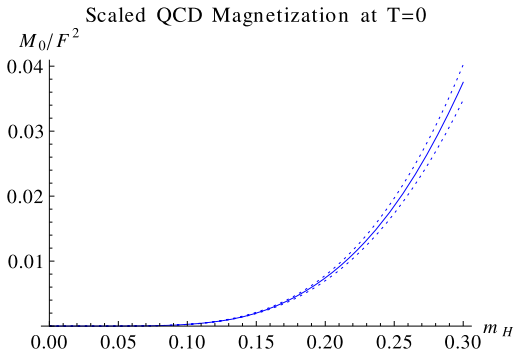

Fig. 1. Scaled zero-temperature QCD magnetization $\mathfrak{M}_0/F^2$ in terms of magnetic field strength (m_H).

system is dominated by the pions that give rise to a negative magnetic susceptibility. However, at more elevated temperatures, spin-$\frac{1}{2}$ and spin-1 hadrons also become important – unlike the pions they yield positive contributions to $\chi_{\rm tot}$. Then, in finite magnetic fields, pions and higher-spin hadrons lead to positive zero-temperature contributions in $\chi_{\rm tot}$ that grow as the magnetic field becomes stronger. Overall, as temperature rises, the system undergoes a qualitative change in its particle content: while hadrons dominate at low temperatures, quarks are the relevant degrees of freedom at high temperatures – in particular, the quark-gluon plasma exhibits strong paramagnetic behavior.

Current lattice QCD simulations and most other studies address the temperature regime around or above $T \approx 110\,\text{MeV}$. An exception is the hadron resonance gas model: much like chiral perturbation theory it applies at low temperatures. However, the study in Ref. [17] was restricted to noninteracting particles. In general, a quantitative investigation of the diamagnetic and paramagnetic phases in finite magnetic fields and at low temperatures, is still lacking. In the present two-flavor CHPT analysis, where pion-pion interactions are taken into account, we provide such a systematic and rigorous low-energy analysis. We derive the two-loop representation for the magnetization and the magnetic susceptibility at zero and finite temperatures in weak external homogeneous magnetic fields. We show that the QCD vacuum at $T = 0$ is paramagnetic in nonzero magnetic fields. In contrast, the finite-temperature portion in the magnetic susceptibility is negative, such that the total magnetic susceptibility χ_{tot} (sum of $T = 0$ and finite-T contribution) may result positive or negative: depending on temperature and magnetic field strength, paramagnetic and diamagnetic phases can be identified in the low-energy region. In zero magnetic field, χ_{tot} is strictly negative in the pion-dominated regime, but as the magnetic field grows, the QCD vacuum turns into a paramagnetic medium at low temperatures. Remarkably, the dependence of χ_{tot} on temperature is non-monotonic in the paramagnetic phase.

It should be pointed out that chiral perturbation theory – as a low-energy effective field theory – starts to break down if one approaches the chiral phase transition that is expected to occur around $T \approx 160\,\text{MeV}$ for two dynamical quark flavors. While in our plots we go up to $T \approx 150\,\text{MeV}$ for illustrative purposes, this caveat should be kept in mind. However, we emphasize that in the region $T \lessapprox 100\,\text{MeV}$ we provide high-precision results in a parameter domain where CHPT is reliable and lattice QCD simulations still are a challenge.

2. Magnetization

We first consider the magnetization that is induced by the external magnetic field. Based on the representation of the renormalized vacuum energy density z_0^H given Eq. (A.10),[3] the magnetization at zero temperature amounts to

$$\mathfrak{M}_0(M_\pi, H) = \frac{|qH|}{8\pi^2}\,\mathcal{J}_{-2} + \frac{M_\pi^2}{16\pi^2}\,\mathcal{J}_{-1} + \frac{\bar{l}_3}{512\pi^4}\,\frac{M_\pi^4}{F^2}\left\{\mathcal{I}_{-1} + \frac{M_\pi^2}{|qH|}\,\mathcal{I}_0\right\} + \frac{\bar{l}_3}{1536\pi^4}\,\frac{M_\pi^2|qH|}{F^2} - \frac{\bar{l}_6 - \bar{l}_5}{768\pi^4}\,\frac{|qH|}{F^2}\left\{3|qH|\mathcal{I}_{-1} + M_\pi^2\mathcal{I}_0\right\}. \tag{2.1}$$

The dimensionless integrals $\mathcal{I}_n(M_\pi, H)$ and $\mathcal{J}_n(M_\pi, H)$, defined in Eq. (A.3), depend on the pion mass M_π and the magnetic field H. The dimensionless quantities $\bar{l}_3, \bar{l}_5, \bar{l}_6$ are so-called next-to-leading order low-energy constants. Following Refs. [35,36], we use the values $\bar{l}_3 = 3.41(82)$ and $\bar{l}_6 - \bar{l}_5 = 2.64 \pm 0.72$. To discuss the properties of the QCD vacuum it is convenient not to use absolute values of M_π, H and T, but to define dimensionless quantities m, m_H, and t as

$$m = \frac{M_\pi}{4\pi F}, \qquad m_H = \frac{\sqrt{|qH|}}{4\pi F}, \qquad t = \frac{T}{4\pi F}. \tag{2.2}$$

The denominator $\Lambda_\chi \approx 4\pi F \approx 1\,\text{GeV}$ is the chiral symmetry breaking scale. For the tree-level pion decay constant we use $F = 85.6\,\text{MeV}$ [36]. At low energies, i.e., in the domain where CHPT is valid, the parameters m, m_H, and t are small. In the subsequent plots we choose $t \lessapprox 0.15$ ($T \lessapprox 150\,\text{MeV}$) and $m_H \lessapprox 0.3$ ($|qH| \lessapprox 0.1\,\text{GeV}^2$). The dependence of $\mathfrak{M}_0(M_\pi, H)$ on magnetic field strength (m_H) is illustrated in Fig. 1 for the physically relevant case $M_\pi = 140\,\text{MeV}$ ($m = 0.130$).[4] Systematic errors in $\mathfrak{M}_0(M_\pi, H)$, Eq. (2.1), arise due to the uncertainties in the low-energy constant $\bar{l}_3$ and the combination $\bar{l}_6 - \bar{l}_5$. These systematic errors are about seven percent at most ($m_H = 0.3$). $\mathfrak{M}_0(M_\pi, H)$

[3] For completeness we provide explicit expressions for the free energy density in Appendix A.

[4] Note that M_π, i.e., the pion mass in the absence of a magnetic field, is set to its physical value 140 MeV by hand. This means that all corrections to the tree-level pion mass M – starting with the one-loop correction given in Eq. (A.4) – are accounted for. No errors are introduced here due to uncertainties in low-energy constants or higher-loop corrections.

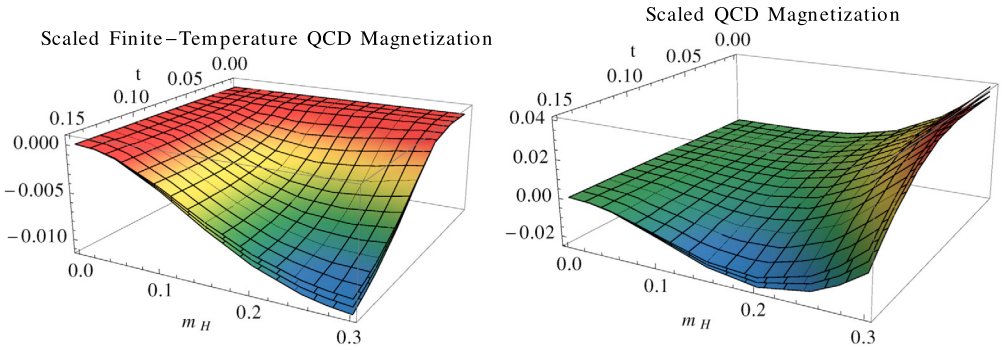

Fig. 2. Scaled finite-temperature QCD magnetization $\mathfrak{M}_T/T^2$ (LHS) and scaled total QCD magnetization $\mathfrak{M}_{tot}/F^2$ (RHS) in terms of magnetic field strength (m_H) and temperature (t).

is positive and grows monotonically as the magnetic field strength increases. The curvature implies paramagnetic behavior. The limit $H \to 0$ does not pose any problems: $\lim_{H\to 0}\mathfrak{M}_0(M_\pi, H) = 0$. As expected, no spontaneous magnetization emerges.

In contrast to $\mathfrak{M}_0(M_\pi, H)$, the purely finite-temperature portion $\mathfrak{M}_T(M_\pi, H)$ in the total magnetization[5]

$$\mathfrak{M}_{\rm tot}(T, M_\pi, H) = \mathfrak{M}_0(M_\pi, H) + \mathfrak{M}_T(M_\pi, H)\,, \tag{2.3}$$

is negative at $M_\pi = 140\,\text{MeV}$ according to the LHS of Fig. 2. Its dependence on T and H is nontrivial: at lower (fixed) temperatures, $|\mathfrak{M}_T(M_\pi, H)|$ initially grows as the magnetic field gets stronger, goes through a maximum and then starts to decline. At fixed magnetic field strength, $|\mathfrak{M}_T(M_\pi, H)|$ also starts to increase less rapidly as temperature rises. With respect to the (negative) one-loop contribution, the two-loop correction is of the order of a few percent and positive, i.e., it slightly weakens the dominant effect. Finally, on the RHS of Fig. 2, we depict the total magnetization which may take positive or negative values. Remarkably, this non-monotonic dependence of $\mathfrak{M}_{tot}(T, M_\pi, H)$ on H implies that the QCD vacuum may behave as a diamagnetic or paramagnetic medium (see below). The systematic errors in the finite-temperature[6] and total magnetization are at most seven percent (LHS of Fig. 2) and up to ten percent (RHS of Fig. 2), respectively. While these errors – due to the uncertainties in low-energy constants – are indicated in the plots, we have not explicitly depicted the other source of errors due to neglected higher-loop corrections. Based on the pioneering CHPT three-loop calculation of the QCD partition function in zero magnetic field, Ref. [38], and based on the general fact that each additional loop correction in CHPT is suppressed by two powers of momentum (energy), these errors are expected to be of the order of a few percent at most.

3. Magnetic susceptibility

We now focus on the magnetic susceptibility where we also present zero-temperature and finite-temperature pieces,

$$\chi_{\rm tot}(T, M_\pi, H) = \chi_0(M_\pi, H) + \chi_T(M_\pi, H)\,, \tag{3.1}$$

separately. The zero-temperature portion reads

$$\begin{aligned}\chi_0(M_\pi, H) = \frac{1}{16\pi^2}\Big\{2\mathcal{J}_{-2} + \frac{2M_\pi^2}{|qH|}\,\mathcal{J}_{-1} + \frac{M_\pi^4}{|qH|^2}\,\mathcal{J}_0\Big\} + \frac{\bar{l}_3}{512\pi^4F^2}\,\frac{M_\pi^8}{|qH|^3}\,\mathcal{I}_1 \\ + \frac{\bar{l}_3}{1536\pi^4}\,\frac{M_\pi^2}{F^2} - \frac{\bar{l}_6-\bar{l}_5}{768\pi^4F^2}\Big\{6|qH|\,\mathcal{I}_{-1} + 4M_\pi^2\,\mathcal{I}_0 + \frac{M_\pi^4}{|qH|}\,\mathcal{I}_1\Big\}\,.\end{aligned} \tag{3.2}$$

According to Appendix B where we analyze the limit $|qH| \ll M_\pi^2$, the corresponding expansion of $\chi_0(M_\pi, H)$ is characterized by even powers of the magnetic field,

$$\chi_0(M_\pi, H) = \alpha_0 + \alpha_2|qH|^2 + \alpha_4|qH|^4 + \mathcal{O}(|qH|^6)\,, \tag{3.3}$$

with coefficients α_n given in Eq. (B.7). As explained in Appendix A.1, we adopt the standard renormalization prescription which is to drop in the $T = 0$ free energy density all terms quadratic in the magnetic field. This means that χ_0 in zero magnetic field is set to zero by definition,

$$\lim_{H\to 0}\chi_0(M_\pi, H) \doteq 0 \qquad \Longleftrightarrow \qquad \alpha_0 \doteq 0\,. \tag{3.4}$$

The dependence of the zero-temperature magnetic susceptibility on magnetic field strength (m_H) at $M_\pi = 140\,\text{MeV}$ is shown in Fig. 3: $\chi_0(M_\pi, H)$ is positive and grows monotonically – the QCD vacuum at $T = 0$ in finite magnetic fields is paramagnetic. Systematic errors due to uncertainties in the low-energy constant $\bar{l}_3$ and the combination $\bar{l}_6 - \bar{l}_5$ are about eight percent at most ($m_H = 0.3$).

[5] The explicit two-loop representation for $\mathfrak{M}_T(M_\pi, H)$ can be found in Ref. [37].

[6] Note that the kinematical functions for the charged pions, Eq. (A.13), depend on the combination $\bar{l}_6 - \bar{l}_5$ of low-energy constants appearing in the charged pion mass, Eq. (A.15). Uncertainties in the low-energy constants then propagate into the analytical kinematical functions and hence into the observables.

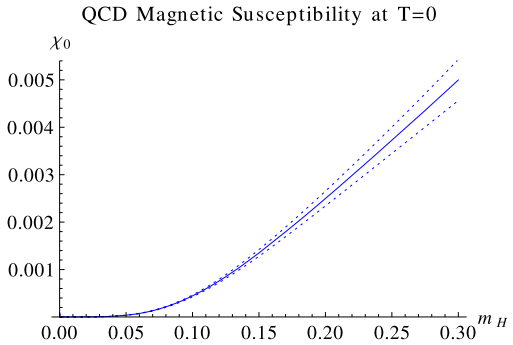

Fig. 3. Zero-temperature QCD magnetic susceptibility χ_0 in terms of magnetic field strength (m_H).

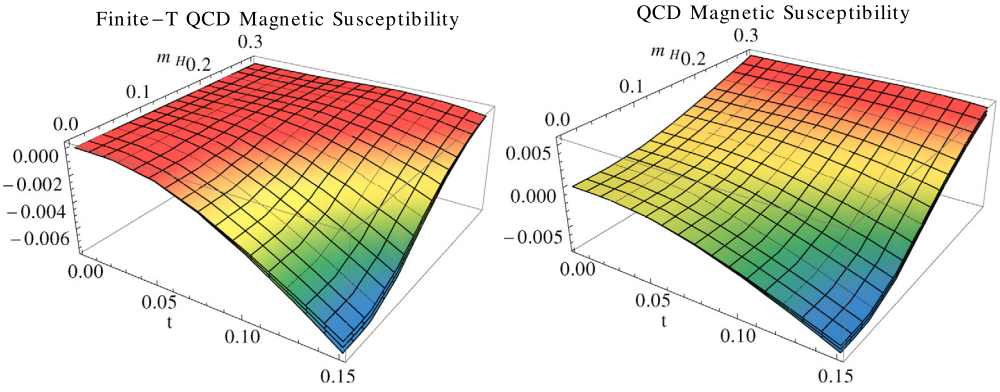

Fig. 4. Finite-temperature QCD magnetic susceptibility χ_T (LHS) and total QCD magnetic susceptibility χ_{tot} (RHS) in terms of magnetic field strength (m_H) and temperature (t).

The finite-temperature portion of the magnetic susceptibility we write as

$$\chi_T(M_\pi, H) = \chi_1(T, M_\pi, H) + \chi_2(T, M_\pi, H)\,. \tag{3.5}$$

The one-loop contribution χ_1 refers to noninteracting pions. The two-loop correction χ_2 contains the pion-pion interaction and is of the order of a few percent compared to χ_1. The respective expressions are rather lengthy and provided in Appendix C. On the LHS of Fig. 4 we depict the dependence of $\chi_T(M_\pi, H)$ on temperature and magnetic field at $M_\pi = 140\,\text{MeV}$: it is negative in most of parameter space accessible by CHPT – only in stronger magnetic fields it takes slightly positive values. At fixed T, $\chi_T(M_\pi, H)$ increases as the magnetic field becomes stronger and then reaches a plateau. At fixed H, overall, $\chi_T(M_\pi, H)$ decreases as temperature rises – however, in stronger magnetic fields, it first slightly grows and then falls off to negative values – hence exhibiting non-monotonic behavior. Systematic errors in the finite-temperature magnetic susceptibility, due to the uncertainties in low-energy constants, are eight percent at most. Additional errors due to neglected higher-loop corrections are expected to be of the order of a few percent.

The main result of the present study concerns the total magnetic susceptibility $\chi_{tot}(T, M_\pi, H)$, i.e., the superposition of $\chi_0(M_\pi, H)$ and $\chi_T(M_\pi, H)$. This quantity indeed exhibits some remarkable features in the low-energy region. First, as we illustrate on the RHS of Fig. 4, in stronger magnetic fields, the QCD vacuum – irrespective of temperature – is *paramagnetic*. In weaker magnetic fields, however, a *diamagnetic* phase starts to emerge – eventually, at $H = 0$, the QCD vacuum is diamagnetic in the entire regime $t < 0.15$ according to our CHPT calculation. Second, the behavior of $\chi_{tot}(T, M_\pi, H)$ in the paramagnetic phase is non-monotonic as can be better appreciated in Fig. 5: as temperature grows – while H kept fixed – χ_{tot} initially rises, goes through a maximum and then starts to drop. It should be pointed out that this phenomenon already emerges at one-loop order and is slightly weakened (of the order of a few permille) by the two-loop correction. The effect is more pronounced in stronger magnetic fields and it is absent at $H = 0$ – in the latter case the QCD vacuum is purely diamagnetic in the pion-dominated low-temperature phase. In the temperature range $t \leq 0.15$, the systematic errors in the total magnetic susceptibility are up to ten percent (RHS of Fig. 4) and eight percent at most (Fig. 5), respectively. Additional errors due to neglected higher-loop corrections, again, are expected of the order of a few percent.

Finally, it is instructive to compare the chiral perturbation theory prediction with alternative approaches. This is indeed possible in the limit $H \to 0$ where HRG model and lattice data are available for the finite-temperature magnetic susceptibility χ_T.[7] In Fig. 6, we plot χ_T at $H = 0$ – in the literature also denoted as $\chi_B(T)$ – for the temperature range $0 \leq t \leq 0.12$ ($0 \leq T \leq 126\,\text{MeV}$). The figure underlines the fact that lattice QCD simulations are a challenge in the low-temperature domain. Directly simulated data points below $T = 90\,\text{MeV}$ appear to be unavailable at present, and the available points in the interval $90\,\text{MeV} \leq T \leq 126\,\text{MeV}$ contain large errors.

However, at higher temperatures (not shown in Fig. 6) lattice data are much more precise. Most important, lattice QCD simulations have demonstrated that the diamagnetic QCD vacuum eventually turns into paramagnetic at higher T. This feature is missed by the HRG model as well as by chiral perturbation theory as they are both restricted to the low-energy (low-temperature) domain. In contrast to two-flavor CHPT, the HRG model – apart from the three pions – takes into account a total of 22 additional particles (see Table 1 of

[7] The author thanks G. Endrődi and G. S. Bali for providing the corresponding data.

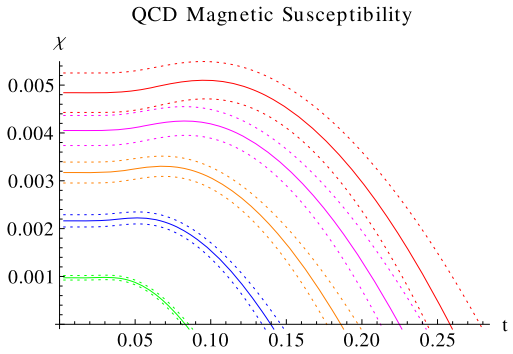

Fig. 5. Non-monotonic behavior of the total QCD magnetic susceptibility in the paramagnetic phase: Dependence of χ_{tot} on temperature (t) at fixed magnetic field strength $|qH| = \{0.02, 0.04, 0.06, 0.08, 0.1\}\,\mathrm{GeV}^2$ (bottom to top).

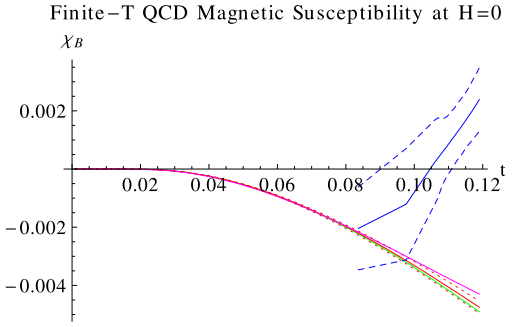

Fig. 6. Temperature dependence of the finite-temperature QCD magnetic susceptibility at $H = 0$: Comparison of different approaches. Lattice data with errors (blue) from Ref. [6], HRG model (magenta) from Ref. [17], and present CHPT analysis: one-loop result (green), two-loop result with systematic errors (red).

Ref. [17]). Still, deviations between the HRG model and CHPT are very small according to Fig. 6, implying that the properties of the system up to temperatures $T \lessapprox 100\,\mathrm{MeV}$ are dominated by the physics of the pions.

4. Conclusions

The subtle interplay between zero-T and finite-T contributions leads to the nontrivial behavior of the magnetization and magnetic susceptibility that we observe at low temperatures and weak magnetic fields. The comparison of CHPT studies of the quark condensate with lattice data performed in Ref. [39] suggests that CHPT is perfectly valid up to magnetic field strengths of $|qH| \lessapprox 0.1\,\mathrm{GeV}^2$ ($m_H \lessapprox 0.3$). Likewise, the HRG model analysis of Ref. [17] concludes that pions no longer dominate at low temperatures beyond $|qH| \gtrapprox 0.2\,\mathrm{GeV}^2$ ($m_H \gtrapprox 0.4$). Our high-precision and fully systematic results for the magnetization and magnetic susceptibility are within this parameter range and thus accurately describe the pion-dominated phase. We hence complement and extend all previous studies on these two observables to a parameter domain that is hardly accessible by lattice QCD at present and has not been examined by any other method beyond leading order in a systematic way. It remains to be seen whether future lattice QCD simulations can quantitatively explore the diamagnetic and paramagnetic phases in the low-energy region of QCD and confirm our predictions.

Declaration of competing interest

The authors declare that they have no known competing financial interests or personal relationships that could have appeared to influence the work reported in this paper.

Acknowledgements

The author thanks G. S. Bali, J. Bijnens, G. Endrődi, and H. Leutwyler for correspondence.

Appendix A. Representation of the free energy density

The purpose of this Appendix is to make the presentation self-contained by providing explicit expressions for the two-loop free energy density z_{tot} which is the starting point of our analysis. It is convenient to split z into two pieces,

$$z_{\mathrm{tot}} = z_0 + z_T\,, \tag{A.1}$$

where z_0 is the free energy density at $T=0$ and z_T is the finite-temperature portion. In what follows we discuss these two pieces individually. The two-loop calculation within the framework of two-flavor chiral perturbation theory[8] in the isospin limit $m_u = m_d$ was performed in Refs. [42,43].

A.1. Zero temperature

The renormalized vacuum energy density z_0 takes the form

$$\begin{aligned} z_0 = &-F^2M^2 + \frac{M^4}{64\pi^2}\Big(\bar{l}_3 - 4\bar{h}_1 - \frac{3}{2}\Big) + \frac{|qH|^2}{96\pi^2}(\bar{h}_2 - 1) - \frac{|qH|^2}{16\pi^2}\mathcal{J}_{-2} \\ &+ \frac{3\bar{l}_3(\bar{c}_{10}+2\bar{c}_{11})}{1024\pi^4}\frac{M^6}{F^2} - \frac{(\bar{l}_6-\bar{l}_5)\bar{c}_{34}}{768\pi^4}\frac{|qH|^2M^2}{F^2} \\ &- \frac{\bar{l}_3}{512\pi^4}\frac{M^4|qH|}{F^2}\mathcal{I}_{-1} + \frac{\bar{l}_6-\bar{l}_5}{768\pi^4}\frac{|qH|^3}{F^2}\mathcal{I}_{-1} + \mathcal{O}(p^8)\,, \end{aligned} \tag{A.2}$$

where the integrals $\mathcal{I}_n$ and $\mathcal{J}_n$ are

$$\begin{aligned} \mathcal{I}_n &= \int_0^\infty \mathrm{d}\rho\, \rho^n \exp\Big(-\frac{M^2}{|qH|}\rho\Big)\Big(\frac{1}{\sinh(\rho)} - \frac{1}{\rho}\Big)\,, \\ \mathcal{J}_n &= \int_0^\infty \mathrm{d}\rho\, \rho^n \exp\Big(-\frac{M^2}{|qH|}\rho\Big)\Big(\frac{1}{\sinh(\rho)} - \frac{1}{\rho} + \frac{\rho}{6}\Big)\,. \end{aligned} \tag{A.3}$$

z_0 contains the renormalized next-to-leading order and next-to-next-to-leading order effective constants, $\bar{l}_3, \bar{l}_5, \bar{l}_6, \bar{h}_1, \bar{h}_2$ and $\bar{c}_{10}, \bar{c}_{11}, \bar{c}_{34}$, respectively. Details on the definition and running of these low-energy couplings can be found in Appendix A of Ref. [43], as well as in the original references [35,44]. Numerical values are provided in the main body of the present paper. Finally, M is the tree-level pion mass which is related to the (one-loop) pion mass M_π as

$$M_\pi^2 = M^2 - \frac{\bar{l}_3}{32\pi^2}\frac{M^4}{F^2} + \mathcal{O}(M^6)\,. \tag{A.4}$$

A crucial question is which contributions in the $T=0$ free energy density are physically relevant. Since we are interested in how the QCD vacuum is affected by the magnetic field, we can ignore all terms that do not involve the magnetic field. We are then left with

$$\begin{aligned} \tilde{z}_0^H = &\frac{|qH|^2}{96\pi^2}(\bar{h}_2 - 1) - \frac{|qH|^2}{16\pi^2}\mathcal{J}_{-2} - \frac{(\bar{l}_6-\bar{l}_5)\bar{c}_{34}}{768\pi^4}\frac{|qH|^2M^2}{F^2} \\ &- \frac{\bar{l}_3}{512\pi^4}\frac{M^4|qH|}{F^2}\mathcal{I}_{-1} + \frac{\bar{l}_6-\bar{l}_5}{768\pi^4}\frac{|qH|^3}{F^2}\mathcal{I}_{-1}\,. \end{aligned} \tag{A.5}$$

Clearly, the contribution

$$-\frac{|qH|^2}{96\pi^2} \tag{A.6}$$

can be dropped as it is independent of the properties of the pions: it does not involve the pion mass, but solely depends on the external magnetic field. Note that there are further terms quadratic in the magnetic field. At chiral order p^4, we have

$$\frac{\bar{h}_2}{96\pi^2}|qH|^2\,, \tag{A.7}$$

and at chiral order p^6 we have

$$-\frac{(\bar{l}_6-\bar{l}_5)\bar{c}_{34}}{768\pi^4}\frac{M^2}{F^2}|qH|^2\,. \tag{A.8}$$

Then – according to the analysis of the integral $\mathcal{I}_{-1}$ in the limit $|qH| \ll M^2$ performed in Appendix B – an additional term quadratic in the magnetic field arises at chiral order p^6, namely,

$$\frac{\bar{l}_3}{3072\pi^4}\frac{M^2}{F^2}|qH|^2\,. \tag{A.9}$$

In order to compare our results with the literature, we adopt the renormalization prescription for the zero-temperature free energy density that underlies lattice as well HRG model studies [1–13,17–19,22], which is to **drop in the $T=0$ free energy density all terms quadratic in the magnetic field**. In our CHPT framework this corresponds to subtracting the terms (A.6)-(A.9) from the vacuum energy density Eq. (A.5). The properly normalized zero-temperature free energy density hence takes the form

[8] Outlines of chiral perturbation theory are given in Refs. [40,41].

$$z_0^H = -\frac{|qH|^2}{16\pi^2}\mathcal{J}_{-2} - \frac{\bar{l}_3}{512\pi^4}\frac{M^4|qH|}{F^2}\Big(\mathcal{I}_{-1} + \frac{|qH|}{6M^2}\Big) + \frac{\bar{l}_6-\bar{l}_5}{768\pi^4}\frac{|qH|^3}{F^2}\mathcal{I}_{-1}\,. \tag{A.10}$$

Note that the difference between the tree-level pion mass M and the one-loop pion mass M_π only starts manifesting itself beyond chiral order p^6. We can therefore safely replace M by M_π in Eq. (A.10). The expansion of z_0^H in the limit $|qH| \ll M^2$ gives rise to even powers of the magnetic field that start at order $|qH|^4$ – all terms quadratic in the magnetic field have been eliminated.[9] Equivalently, within this convention, the $T = 0$ magnetic susceptibility χ_0 in zero magnetic field is set to zero by definition,

$$\lim_{H\to 0}\chi_0 = \lim_{H\to 0} -\frac{\mathrm{d}^2 z_0^H}{\mathrm{d}|qH|^2} \doteq 0\,. \tag{A.11}$$

It is important to emphasize that our assessment of whether the QCD vacuum has diamagnetic or paramagnetic properties is tied to this renormalization convention.

A.2. Finite temperature

For completeness we provide the finite-temperature contribution z_T in the free energy density. Following Ref. [42], the two-loop representation reads

$$\begin{aligned} z_T = &-g_0(M_\pi^\pm, T, 0) - \frac{1}{2}g_0(M_\pi^0, T, 0) - \tilde{g}_0(M_\pi^\pm, T, H) \\ &+\frac{M_\pi^2}{2F^2}\,g_1(M_\pi^\pm, T, 0)\,g_1(M_\pi^0, T, 0) - \frac{M_\pi^2}{8F^2}\Big\{g_1(M_\pi^0, T, 0)\Big\}^2 \\ &+\frac{M_\pi^2}{2F^2}\,g_1(M_\pi^0, T, 0)\,\tilde{g}_1(M_\pi^\pm, T, H) + \mathcal{O}(p^8)\,, \end{aligned} \tag{A.12}$$

with respective Bose functions defined as

$$\begin{aligned} g_r(\mathcal{M}, T, 0) &= \frac{T^{4-2r}}{(4\pi)^r}\int_0^\infty \mathrm{d}\rho\,\rho^{r-3}\,\exp\Big(-\frac{\mathcal{M}^2}{4\pi T^2}\rho\Big)\Big[S\Big(\frac{1}{\rho}\Big) - 1\Big]\,, \\ \tilde{g}_r(M_\pi^\pm, T, H) &= \frac{T^{2-2r}}{(4\pi)^{r+1}}\,|qH|\int_0^\infty \mathrm{d}\rho\,\rho^{r-2}\left(\frac{1}{\sinh(|qH|\rho/4\pi T^2)} - \frac{4\pi T^2}{|qH|\rho}\right) \\ &\quad\times \exp\Big(-\frac{(M_\pi^\pm)^2}{4\pi T^2}\rho\Big)\Big[S\Big(\frac{1}{\rho}\Big) - 1\Big]\,, \end{aligned} \tag{A.13}$$

where $S(z)$,

$$S(z) = \sum_{n=-\infty}^{\infty}\exp(-\pi n^2 z)\,, \tag{A.14}$$

is the Jacobi theta function. The Bose functions involve the quantities $M_\pi^\pm$ and M_π^0, i.e., the masses of the charged and neutral pions subjected to the magnetic field,

$$\begin{aligned} (M_\pi^\pm)^2 &= M_\pi^2 + \frac{\bar{l}_6-\bar{l}_5}{48\pi^2}\frac{|qH|^2}{F^2}\,, \\ (M_\pi^0)^2 &= M_\pi^2 + \frac{M^2|qH|}{16\pi^2F^2}\mathcal{I}_{-1}\,. \end{aligned} \tag{A.15}$$

The symbol $\mathcal{M}$ in the kinematical Bose functions g_r can either denote $M_\pi^\pm$ or M_π^0 depending on context. The quantity M_π is the (one-loop) pion mass in zero magnetic field defined by Eq. (A.4).

Appendix B. Zero-temperature magnetic susceptibility in the limit $|qH| \ll M^2$

In this Appendix we identify the structure of magnetic field powers in the zero-temperature magnetic susceptibility $\chi_0(M, H)$ by considering the limit $|qH| \ll M^2$. The quantity $\chi_0(M, H)$,

$$\chi_0(M, H) = -\frac{\mathrm{d}^2 z_0}{\mathrm{d}|qH|^2}\,, \tag{B.1}$$

with z_0 given in Eq. (A.2), contains the integrals $\mathcal{I}_n$ and $\mathcal{J}_n$ – see Eq. (A.3) – that we write as

[9] This means that the NLO effective constant $\bar{h}_2$ and the NNLO effective constant $\bar{c}_{34}$ are irrelevant within the adopted renormalization prescription.

$$\mathcal{I}_n = \varepsilon^{n+1} \int_0^\infty \mathrm{d}\rho\, \rho^n\, e^{-\rho} \left(\frac{1}{\sinh(\varepsilon\rho)} - \frac{1}{\varepsilon\rho} \right),$$
$$\mathcal{J}_n = \varepsilon^{n+1} \int_0^\infty \mathrm{d}\rho\, \rho^n\, e^{-\rho} \left(\frac{1}{\sinh(\varepsilon\rho)} - \frac{1}{\varepsilon\rho} + \frac{\varepsilon\rho}{6} \right), \tag{B.2}$$

where ε,

$$\varepsilon = \frac{|qH|}{M^2}, \tag{B.3}$$

is the relevant expansion parameter. The integrands yield the series

$$\frac{1}{\sinh(\varepsilon\rho)} - \frac{1}{\varepsilon\rho} = \hat{c}_1 \rho\, \varepsilon + \hat{c}_2 \rho^3 \varepsilon^3 + \hat{c}_3 \rho^5 \varepsilon^5 + \mathcal{O}(\varepsilon^7), \tag{B.4}$$

with the first five Taylor coefficients as

$$\begin{aligned}
\hat{c}_1 &= -\frac{1}{6} \approx -0.167, \\
\hat{c}_2 &= \frac{7}{360} \approx 0.0194, \\
\hat{c}_3 &= -\frac{31}{15120} \approx -0.00205, \\
\hat{c}_4 &= \frac{127}{604800} \approx 0.000210, \\
\hat{c}_5 &= -\frac{73}{3421440} \approx -0.0000213.
\end{aligned} \tag{B.5}$$

Collecting terms, we find that the zero-temperature magnetic susceptibility features even powers of the magnetic field and amounts to

$$\chi_0(M,H) = \alpha_0 + \alpha_2 |qH|^2 + \alpha_4 |qH|^4 + \mathcal{O}(|qH|^6), \tag{B.6}$$

with respective coefficients

$$\begin{aligned}
\alpha_0 &= -\frac{\overline{h}_2 - 1}{48\pi^2} + \frac{\overline{c}_{34}(\bar{l}_6 - \bar{l}_5)}{384\pi^4} \frac{M^2}{F^2} - \frac{\bar{l}_3}{1536\pi^4} \frac{M^2}{F^2}, \\
\alpha_2 &= \frac{7}{480\pi^2 M^4} + \frac{7\bar{l}_3}{7680\pi^4 F^2 M^2} + \frac{\bar{l}_6 - \bar{l}_5}{384\pi^4 F^2 M^2}, \\
\alpha_4 &= -\frac{31}{1344\pi^2 M^8} - \frac{31\bar{l}_3}{10752\pi^4 F^2 M^6} - \frac{7(\bar{l}_6 - \bar{l}_5)}{4608\pi^4 F^2 M^6}.
\end{aligned} \tag{B.7}$$

Again we point out that the renormalization convention adapted for the $T = 0$ free energy density specified in Appendix A.1 implies that the coefficient α_0 is set to zero by definition, i.e., the contribution α_0 is subtracted from the zero-temperature magnetic susceptibility $\chi_0(M,H)$.

Appendix C. Magnetic susceptibility at finite temperature

Here we provide the explicit representation of the finite-temperature magnetic susceptibility – χ_T – in terms of the various kinematical Bose functions involved.[10] In the derivation of χ_T,

$$\chi_T = -\frac{\mathrm{d}^2 z_T}{\mathrm{d}|qH|^2}, \tag{C.1}$$

the following identities featuring derivatives of Bose functions with respect to the magnetic field are useful,

$$\begin{aligned}
\frac{\mathrm{d}}{\mathrm{d}|qH|}\, g_r(M_\pi^\pm, T, 0) &= -\frac{\bar{l}_6 - \bar{l}_5}{24\pi^2} \frac{|qH|}{F^2}\, g_{r+1}(M_\pi^\pm, T, 0), \\
\frac{\mathrm{d}}{\mathrm{d}|qH|}\, g_r(M_\pi^0, T, 0) &= -\frac{M_\pi^2}{16\pi^2 F^2} \left(\mathcal{I}_{-1} + \frac{M_\pi^2}{|qH|} \mathcal{I}_0 \right) g_{r+1}(M_\pi^0, T, 0), \\
\frac{\mathrm{d}}{\mathrm{d}|qH|}\, \tilde{g}_r(M_\pi^\pm, T, H) &= \frac{1}{|qH|}\, \tilde{g}_r(M_\pi^\pm, T, H) - \frac{\bar{l}_6 - \bar{l}_5}{24\pi^2} \frac{|qH|}{F^2}\, \tilde{g}_{r+1}(M_\pi^\pm, T, H) + \tilde{g}_r^{[H]}(M_\pi^\pm, T, H),
\end{aligned} \tag{C.2}$$

where

[10] The Bose functions g_r and $\tilde{g}_r$ are defined in Eq. (A.13).

$$\tilde{g}_r^{[H]}(M_\pi^\pm,T,H)=\frac{T^{2-2r}}{(4\pi)^{r+1}}\,|qH|\int_0^\infty \mathrm{d}\rho\rho^{r-2}\left(-\frac{\rho\coth(|qH|\rho/4\pi T^2)}{4\pi T^2\sinh(|qH|\rho/4\pi T^2)}+\frac{4\pi T^2}{|qH|^2\rho}\right)$$
$$\times\exp\Big(-\frac{(M_\pi^\pm)^2}{4\pi T^2}\rho\Big)\bigg[S\Big(\frac{1}{\rho}\Big)-1\bigg]. \tag{C.3}$$

Instead of using dimensionful Bose functions g_r and $\tilde{g}_r$, it is more transparent to express observables by dimensionless Bose functions h_r and $\tilde{h}_r$,

$$h_0=\frac{g_0}{T^4}\,,\quad \tilde{h}_0=\frac{\tilde{g}_0}{T^4}\,,\qquad h_1=\frac{g_1}{T^2}\,,\quad \tilde{h}_1=\frac{\tilde{g}_1}{T^2}\,,\qquad h_2=g_2\,,\quad \tilde{h}_2=\tilde{g}_2\,. \tag{C.4}$$

The finite-temperature magnetic susceptibility χ_T can then be written in the form

$$\chi_T(M_\pi,H)=\chi_1(T,M_\pi,H)+\chi_2(T,M_\pi,H)\,. \tag{C.5}$$

One-loop and two-loop contributions, respectively, are

$$\chi_1=\frac{m_\pm t^2}{m_H^2}\,h_1(M_\pi^\pm,T,0)+m_\pm^2\,h_2(M_\pi^\pm,T,0)+\frac{t^2}{4m_H}\,\chi_0\,h_1(M_\pi^0,T,0)$$
$$+\frac{m_0^2}{2}\,h_2(M_\pi^0,T,0)+\frac{3m_\pm t^2}{m_H^2}\,\tilde{h}_1(M_\pi^\pm,T,H)+\frac{t^2}{m_H^2}\,\tilde{h}_0^{[H]}(M_\pi^\pm,T,H)$$
$$+\frac{t^2}{2m_H}\,\frac{\mathrm{d}}{\mathrm{d}m_H}\,\tilde{h}_0^{[H]}(M_\pi^\pm,T,H)+m_\pm^2\tilde{h}_2(M_\pi^\pm,T,H)+m_\pm\tilde{h}_1^{[H]}(M_\pi^\pm,T,H)\,,$$
$$\chi_2=8\pi^2m^2\bigg\{-\frac{t^2}{m_H^2}\,m_\pm h_2(M_\pi^\pm,T,0)h_1(M_\pi^0,T,0)-m_\pm^2h_3(M_\pi^\pm,T,0)h_1(M_\pi^0,T,0)$$
$$-2m_\pm m_0h_2(M_\pi^\pm,T,0)h_2(M_\pi^0,T,0)-\frac{t^2}{2m_H}\,\chi_0\,h_1(M_\pi^\pm,T,0)h_2(M_\pi^0,T,0)$$
$$-m_0^2h_1(M_\pi^\pm,T,0)h_3(M_\pi^0,T,0)-\frac{t^2}{2m_H}\,\chi_0\,h_2(M_\pi^0,T,0)\tilde{h}_1(M_\pi^\pm,T,H)$$
$$-m_0^2h_3(M_\pi^0,T,0)\tilde{h}_1(M_\pi^\pm,T,H)-\frac{2t^2}{m_H^2}\,m_0h_2(M_\pi^0,T,0)\tilde{h}_1(M_\pi^\pm,T,H)$$
$$-m_0m_\pm h_2(M_\pi^0,T,0)\tilde{h}_2(M_\pi^\pm,T,H)-2m_0h_2(M_\pi^0,T,0)\tilde{h}_1^{[H]}(M_\pi^\pm,T,H)$$
$$-\frac{2t^2}{m_H^2}\,m_\pm\,h_1(M_\pi^0,T,0)\tilde{h}_2(M_\pi^\pm,T,H)-\frac{t^2}{m_H^2}\,h_1(M_\pi^0,T,0)\tilde{h}_1^{[H]}(M_\pi^\pm,T,H)$$
$$-m_\pm^2h_1(M_\pi^0,T,0)\tilde{h}_3(M_\pi^\pm,T,H)-m_\pm h_1(M_\pi^0,T,0)\tilde{h}_2^{[H]}(M_\pi^\pm,T,H)$$
$$-\frac{t^2}{2m_H}\,h_1(M_\pi^0,T,0)\frac{\mathrm{d}}{\mathrm{d}m_H}\,\tilde{h}_1^{[H]}(M_\pi^\pm,T,H)+\frac{m_0^2}{2}\,h_3(M_\pi^0,T,0)h_1(M_\pi^0,T,0)$$
$$+\frac{t^2}{4m_H}\,\chi_0\,h_2(M_\pi^0,T,0)h_1(M_\pi^0,T,0)+\frac{m_0^2}{2}\,h_2(M_\pi^0,T,0)h_2(M_\pi^0,T,0)\bigg\}, \tag{C.6}$$

with coefficients

$$m_\pm=-\frac{2(\bar{l}_6-\bar{l}_5)m_H^2}{3}\,,$$
$$m_0=-m^2\int_0^\infty \mathrm{d}\rho\,\rho^{-1}\,\exp\Big(-\frac{m^2}{m_H^2}\rho\Big)\Big(\frac{1}{\sinh(\rho)}-\frac{1}{\rho}\Big)$$
$$-\frac{m^4}{m_H^2}\int_0^\infty \mathrm{d}\rho\,\exp\Big(-\frac{m^2}{m_H^2}\rho\Big)\Big(\frac{1}{\sinh(\rho)}-\frac{1}{\rho}\Big),$$
$$\chi_0=-\frac{2m^6}{m_H^5}\int_0^\infty \mathrm{d}\rho\,\rho\,\exp\Big(-\frac{m^2}{m_H^2}\rho\Big)\Big(\frac{1}{\sinh(\rho)}-\frac{1}{\rho}\Big). \tag{C.7}$$

The dimensionless functions $\tilde{h}_r^{[H]}(M_\pi^\pm,T,H)$ read

$$\tilde{h}_0^{[H]}(M_\pi^\pm, T, H) = \frac{\tilde{g}_0^{[H]}(M_\pi^\pm, T, H)}{T^2}\,, \qquad \tilde{h}_1^{[H]}(M_\pi^\pm, T, H) = \tilde{g}_1^{[H]}(M_\pi^\pm, T, H)\,,$$
$$\tilde{h}_2^{[H]}(M_\pi^\pm, T, H) = \tilde{g}_2^{[H]}(M_\pi^\pm, T, H)\ \times T^2\,, \tag{C.8}$$

while h_3 and $\tilde{h}_3$ are

$$h_3 = g_3\, T^2\,, \quad \tilde{h}_3 = \tilde{g}_3\, T^2\,. \tag{C.9}$$

References

[1] G.S. Bali, F. Bruckmann, M. Constantinou, M. Costa, G. Endrődi, S.D. Katz, H. Panagopoulos, A. Schäfer, Phys. Rev. D 86 (2012) 094512.
[2] C. Bonati, M. D'Elia, M. Mariti, F. Negro, F. Sanfilippo, Phys. Rev. Lett. 111 (2013) 182001.
[3] G.S. Bali, F. Bruckmann, G. Endrődi, F. Gruber, A. Schäfer, J. High Energy Phys. 04 (2013) 130.
[4] G.S. Bali, F. Bruckmann, G. Endrődi, A. Schäfer, PoS LATTICE2013 (2013) 182.
[5] C. Bonati, M. D'Elia, M. Mariti, F. Negro, F. Sanfilippo, PoS LATTICE2013 (2013) 184.
[6] G.S. Bali, F. Bruckmann, G. Endrődi, S.D. Katz, A. Schäfer, J. High Energy Phys. 08 (2014) 177.
[7] C. Bonati, M. D'Elia, M. Mariti, F. Negro, F. Sanfilippo, Phys. Rev. D 89 (2014) 054506.
[8] G.S. Bali, F. Bruckmann, G. Endrődi, A. Schäfer, Phys. Rev. Lett. 112 (2014) 042301.
[9] L. Levkova, C. DeTar, Phys. Rev. Lett. 112 (2014) 012002.
[10] G. Endrődi, PoS CPOD2014 (2014) 038.
[11] C. Bonati, M. D'Elia, M. Mariti, M. Mesiti, F. Negro, F. Sanfilippo, PoS LATTICE2014 (2014) 237.
[12] V.V. Braguta, M.N. Chernodub, A.Y. Kotov, A.V. Molochkov, A.A. Nikolaev, Phys. Rev. D 100 (2019) 114503.
[13] G.S. Bali, G. Endrődi, S. Piemonte, J. High Energy Phys. 07 (2020) 183.
[14] S. Fayazbakhsh, N. Sadooghi, Phys. Rev. D 90 (2014) 105030.
[15] V.P. Pagura, D. Gómez Dumm, S. Noguera, N.N. Scoccola, Phys. Rev. D 94 (2016) 054038.
[16] R.L.S. Farias, V.S. Timóteo, S.S. Avancini, M.B. Pinto, G. Krein, Eur. Phys. J. A 53 (2017) 101.
[17] G. Endrődi, J. High Energy Phys. 04 (2013) 023.
[18] A.N. Tawfik, A.M. Diab, N. Ezzelarab, A.G. Shalaby, Adv. High Energy Phys. 2016 (2016) 1381479.
[19] G. Kadam, S. Pal, A. Bhattacharyya, arXiv:1908.10618.
[20] D. Kabat, K. Lee, E. Weinberg, Phys. Rev. D 66 (2002) 014004.
[21] A.N. Tawfik, N. Magdy, Phys. Rev. C 90 (2014) 015204.
[22] T. Steinert, W. Cassing, Phys. Rev. C 89 (2014) 035203.
[23] K. Kamikado, T. Kanazawa, J. High Energy Phys. 01 (2015) 129.
[24] Y.A. Simonov, V.D. Orlovsky, JETP Lett. 101 (2015) 423.
[25] V.D. Orlovsky, Y.A. Simonov, Int. J. Mod. Phys. A 30 (2015) 1550060.
[26] Y. Tsue, J. da Providencia, C. Providencia, M. Yamamura, H. Bohr, Prog. Theor. Exp. Phys. (2015) 103D01.
[27] A.N. Tawfik, A.M. Diab, M.T. Hussein, arXiv:1604.08174.
[28] M.A. Andreichikov, Y.A. Simonov, Eur. Phys. J. C 78 (2018) 420.
[29] A.N. Tawfik, A.M. Diab, M.T. Hussein, J. Exp. Theor. Phys. 126 (2018) 620.
[30] X. Li, W. Fu, Y. Liu, Phys. Rev. D 99 (2019) 074029.
[31] B. Karmakar, R. Ghosh, A. Bandyopadhyay, N. Haque, M.G. Mustafa, Phys. Rev. D 99 (2019) 094002.
[32] S. Rath, B.K. Patra, Eur. Phys. J. A 55 (2019) 220.
[33] S.S. Avancini, R.L.S. Farias, M.B. Pinto, T.E. Restrepo, W.R. Tavares, arXiv:2008.10720.
[34] P. Adhikari, J.O. Andersen, arXiv:2102.01080, 2021.
[35] J. Gasser, H. Leutwyler, Ann. Phys. (N.Y.) 158 (1984) 142.
[36] S. Aoki, et al., Eur. Phys. J. C 80 (2020) 113.
[37] C.P. Hofmann, arXiv:2012.06461, 2020.
[38] P. Gerber, H. Leutwyler, Nucl. Phys. B 321 (1989) 387.
[39] G.S. Bali, F. Bruckmann, G. Endrődi, Z. Fodor, S.D. Katz, A. Schäfer, Phys. Rev. D 86 (2012) 071502(R).
[40] H. Leutwyler, in: V.E. Herscovitz, C.A.Z. Vasconcellos, E. Ferreira (Eds.), Hadron Physics 94 – Topics on the Structure and Interaction of Hadronic Systems, World Scientific, Singapore, 1995, p. 1.
[41] S. Scherer, Adv. Nucl. Phys. 27 (2003) 277.
[42] C.P. Hofmann, Phys. Rev. D 101 (2020) 114031.
[43] C.P. Hofmann, Phys. Rev. D 102 (2020) 094010.
[44] J. Bijnens, G. Colangelo, G. Ecker, Ann. Phys. (N.Y.) 280 (2000) 100.